Interpretation of the hydrogen effect on the static and dynamic tensile behaviour of dual phase steel

T. DEPOVER (1) , F. VERCRUYSSE (2) , A. ELMAHDY (2) , P. VERLEYSEN (2) , K. VERBEKEN (1)

(1) Department of Materials, Textiles and Chemical Engineering, Ghent University (UGent), Technologiepark 903, B-9052 Ghent, Belgium

(2) Department of Electrical Energy, Metals, Mechanical Constructions & Systems, Ghent University (UGent), Technologiepark 903, B-9052 Zwijnaarde, Belgium

ABSTRACT

Present work considers the hydrogen (H) induced mechanical degradation in a dual phase steel by performing tensile tests under static and dynamic conditions. Tensile specimens were electrochemically H pre-charged until saturation and tensile tests were subsequently executed ex-situ. The applied current density was modified to induce different H contents into the samples. The impact of H diffusivity during the tensile tests on the hydrogen embrittlement (HE) susceptibility was evaluated by increasing the strain rate from static ($1.67*10^{-2}$ and 1.67 s^{-1}) to dynamic (450 and 900 s^{-1}) conditions. Additionally, the experiments allow assessing the possibly detrimental effect of the combination of dynamic loading and H on the mechanical response of DP steel. Therefore, a reproducible methodology was established to deliver reliable and innovative data. A standardized tensile machine was used for static testing while split Hopkinson bar experiments were performed for dynamic conditions. The HE resistance decreased when current density increased for all strain rates due to higher H amounts in the sample, as confirmed by melt extraction. The HE% increased when slower strain rates were applied since H was able to diffuse to a crack tip and hence accelerate failure. Even at the highest strain rate (900 s^{-1}), the material lost about 10% of its ductility. However, this observation was related with H in the material and not with H diffusion during testing. This was concluded since H induced brittle failure initiated at the edges of the samples at slow strain rates. Though at a strain rate of 1.67 s^{-1}, fracture initiated in a ductile way from the center similarly as tests performed without pre-charging. Fractography on fracture surfaces revealed a brittle central line when charged with H, which evolved into a major crack. EDX analysis showed MnS inclusions were present in this central line, affecting H induced crack initiation.

KEYWORDS

hydrogen embrittlement
hydrogen diffusivity
static and dynamic tensile testing
Hopkinson
dual phase steel.

INTRODUCTION

High strength steels (HSS), such as for instance dual phase (DP) steels, are widely used within the automotive industry due to their excellent combination of both strength and formability. Their use has even been encouraged since they can both guarantee an increased safety together with weight reduction which is required to meet the stringent CO_2 emissions regulations. DP steel has a ferrite-martensite microstructure with low yield strength, but a high work hardening exponent at low and moderate deformation levels leading to a high ultimate tensile strength. The typical characteristics of DP steel are determined by the thermo-mechanical processing and the volume fraction of austenite islands that transform into martensite. The strength level is primarily dependent on the volume fraction and hardness of the martensite in the DP structure.

Unfortunately, HSS steels are considered to be sensitive to hydrogen (H) induced mechanical degradation, which hinders further alloy development [1]. Basically, these materials suffer, in the presence of H, from a large ductility loss, referred to as hydrogen embrittlement (HE). Amongst others, DP, transformation induced plasticity (TRIP) and high strength low alloyed (HSLA) steels are commonly used grades in the automotive industry and were already subject of multiple H related studies [2,3,4,5,6,7]. The impact of H on the mechanical properties was specifically studied in [8]. A low degree of HE of about 8% was obtained for the HSLA steel due to the presence of Ti and Nb carbonitrides, whereas DP and TRIP steel embrittled with 54% and 60%, respectively. Duprez *et al.* [9] performed tensile tests on these materials immediately after electrochemical H charging and on samples that were atmospherically discharged for one week. They concluded that the H induced ductility loss for DP and TRIP steel was reversible since a large part of the ductility was recovered after discharging for one week, whereas the difference between immediate and after one week testing was limited for HSLA. These observations were correlated with the findings by Escobar *et al.* [10], who performed a thermal desorption spectroscopy (TDS) study on these high strength steels. Different times in vacuum, before the TDS measurement started, were applied and they observed that H present in TRIP and DP steel was mainly diffusible, leaving the material easily when in vacuum, whereas the opposite observations were made for HSLA.

The significant mechanical contrast between the two phases in DP steels introduces certain jeopardies, especially in the presence of H [11]. Gu *et al.* [12] considered the delayed fracture properties of a H charged 1500 MPa bainite-martensite DP steel and revealed that its crack growth rate is less than that of conventional quenched and tempered high strength steels. They ascribed this to the fine DP microstructure and the lath boundaries which may act as beneficial H traps, slowing down segregation and diffusion of H to the crack tip. However, Sun *et al.* [13], attributed the relative high sensitivity of DP steels to HE to sub-structural changes, because cracks initiated along the interface and lath boundaries when H charging was applied. Recently, Koyama *et al.* [14] studied the micro-cracking behavior in martensite-ferrite DP in the presence of H. They demonstrated that H affected the damage evolution process considerably. Both the H-enhanced decohesion (HEDE) and H-enhanced localized plasticity (HELP) mechanisms were considered to contribute to the damage evolution in DP steels leading to an unpredictable HE failure. The impact of H diffusion was recently visualized in DP steel by studying the fracture surfaces of an in-situ charged tensile specimen [15]. The calculated H diffusion distance matched perfectly with the observed transition between H induced brittle and ductile fracture.

Nevertheless, HSS are still often used in body-in-white vehicle structures due to their weight reducing capacity. Crashworthiness is a key parameter of these structures and many mechanical parameters are strain rate dependent. The combination of HE and dynamic high strain rate conditions has not yet been given much attention so far. The aim of this work is to get a better understanding on the role of H in a specific DP steel grade. The influence of H was investigated by modifying both the H content and the applied strain rate from static to dynamic conditions.

EXPERIMENTAL PROCEDURE

MATERIAL CHARACTERIZATION

The H induced mechanical degradation of a DP600 steel was studied in this work. Hot and cold rolling was done till a thickness of 1.2 mm, followed by subsequent annealing via industrial annealing parameters required attaining the desired microstructure. The chemical composition is presented in Table 1.

Table 1 - Chemical composition of the used materials in wt%.

Material/Element	C	Mn	Si	Other
DP	0.07	1.50	0.25	0.4%-0.8% Cr + Mo

The samples were ground using a Ziersch and Baltrusch surface grinder. After grinding, tensile samples were machined, the tensile axis being parallel to the rolling direction. A dogbone-shaped specimen geometry was used (cf. Figure 1). The microstructure was characterized using light optical microscopy (LOM). First the material was grinded and polished, then it was etched using a 2% Nital solution and samples were immediately cleaned using methanol and acetone. The DP600 steel is a ferritic-martensitic dual phase steel with approximately 23.6% of martensite and a grain size of about 7 mm for the ferritic phase and about 2 mm for the martensitic phase, as displayed in Figure 2.

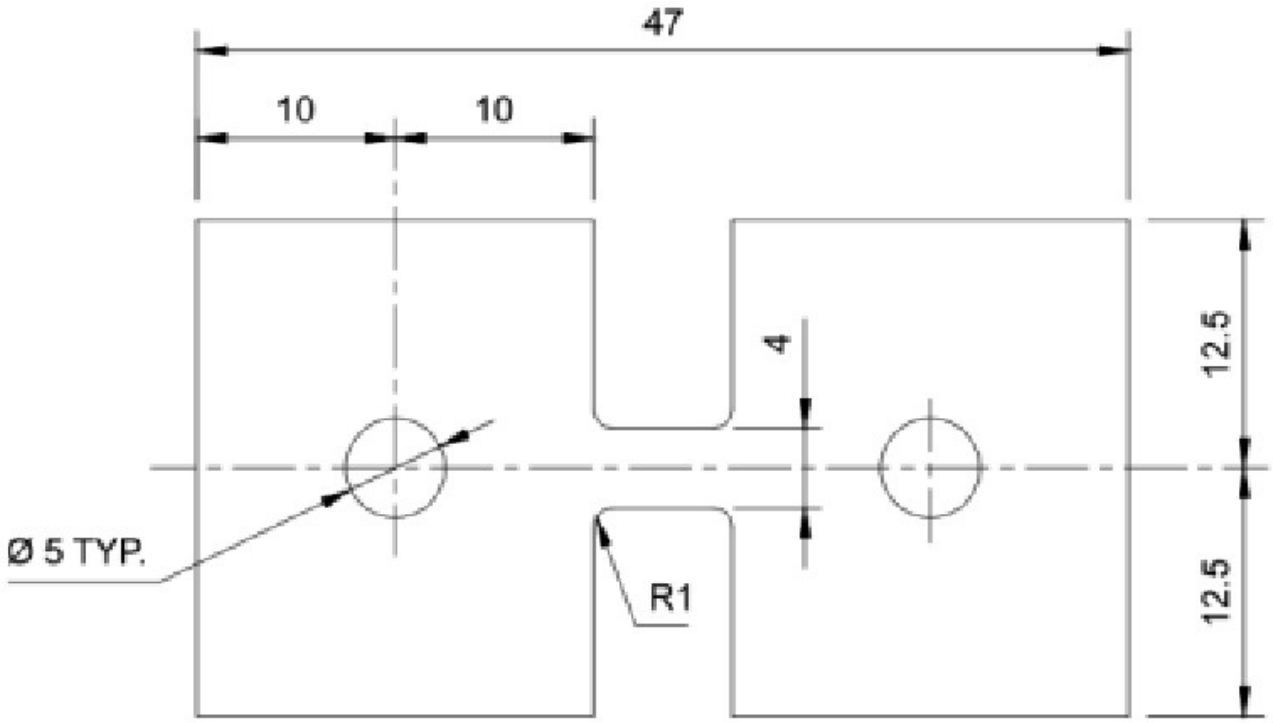

Figure 1 - Tensile sample geometry in mm.

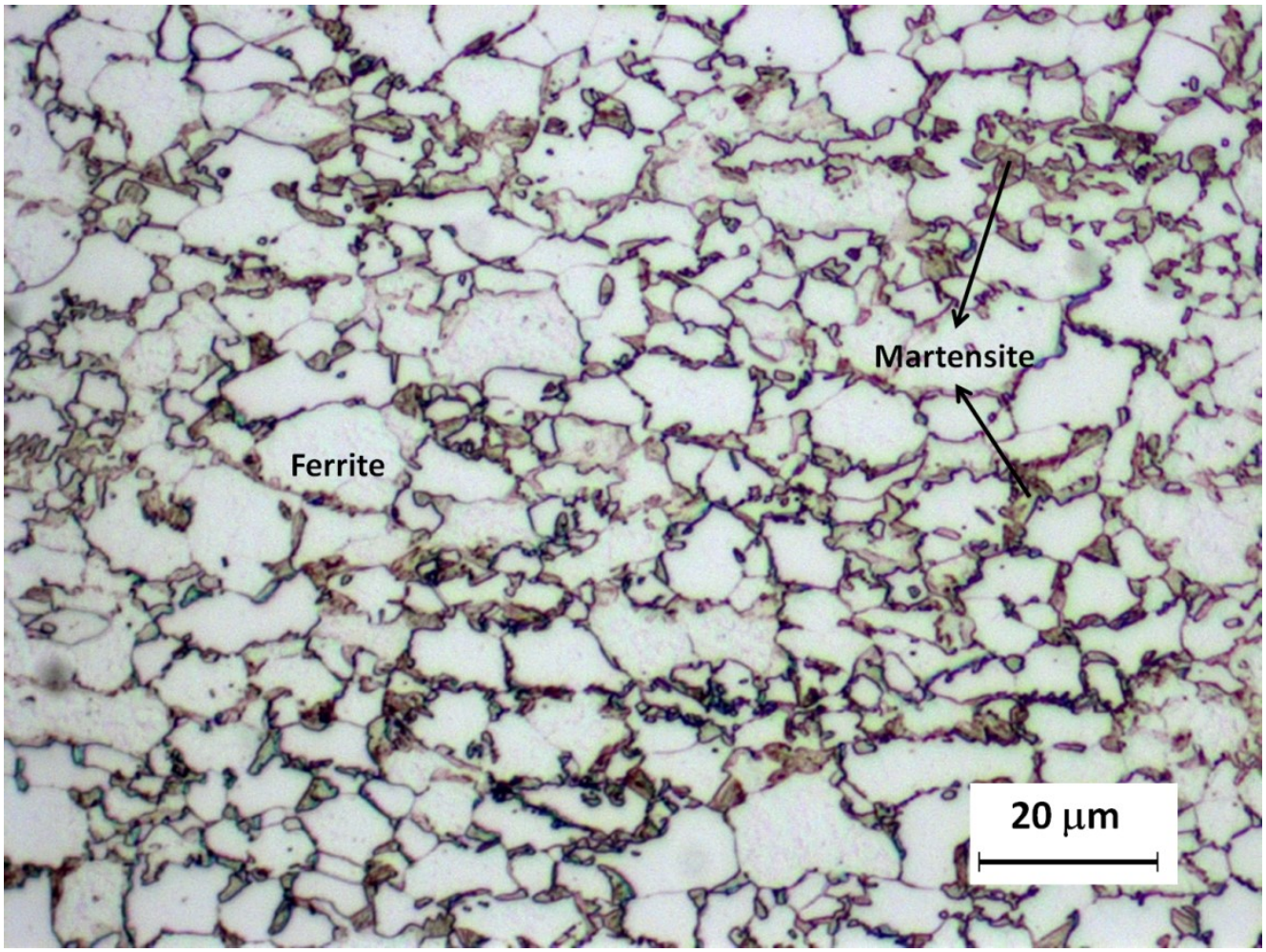

Figure 2 - Optical microscopic image of DP600 steel.

DETERMINATION OF TOTAL HYDROGEN CONTENT

To determine the total H content, melt extraction was used at 1600°C, for which samples were charged electrochemically in 1 g/l thiourea 0.5 M H_2SO_4 electrolyte for two hours. The applied current density was modified in order to induce different amounts of H into the samples. For absorption from an aqueous solution, a relation is found between H absorption and the applied current density during electrochemical charging, i.e. the solubility is proportional to the square root of the current density [16]. The used current densities increased from 0.8 - 5 - 25 mA/cm^2. The time between H pre-charging and the H detection was kept constant at 2 minutes due to the experimental developed procedure to perform both the static and dynamic tensile tests. The system includes a pulse furnace in which a pre-weighted sample is heated directly to the required temperature. The metallic sample releases its H as gaseous H_2 and is dragged along by a nitrogen flow. This mixture (N_2–H_2) is directed to a thermal conductivity measuring cell. Essentially, the thermal conductivity of the mixture depends on the H_2 concentration since the conductivity of H_2 and N_2 differs significantly. As such, the software can calculate the H concentration based on the variation in thermal conductivity.

DETERMINATION OF THE HYDROGEN INDUCED MECHANICAL DEGRADATION

The H induced ductility loss was studied by performing tensile tests on uncharged and H pre-charged samples while using the abovementioned charging parameters. The H impact was quantified by the HE% (cf. Eq. (1)), with ε_{ch} and ε_{un} being the engineering strains averaged over the sample gauge section of the H pre-charged and uncharged sample, respectively. Hence,

the HE degree can vary between 0 and 1, with 0 indicating no ductility drop and insensitivity to HE. When an index of 1 is obtained, the ductility drop is 100% and the HE is maximal.

$$\%\,HE = 100\,(1 - \frac{\varepsilon_{ch}}{\varepsilon_{un}}) \quad (1)$$

First of all, HE was studied by static tensile tests performed on both uncharged and H pre-charged specimens. It must be mentioned that H pre-charging was done for two hours and tensile tests were executed ex-situ due to experimental requirements. A constant time lag of 2 minutes between H pre-charging and tensile testing was maintained. The observations were correlated with those obtained by the melt extraction, which was also done after 2 minutes of H pre-charging. At first, these static tensile tests were done after H pre-charging at different applied current densities to evaluate the impact of the H content on the HE susceptibility. Secondly, the effect of H diffusivity was verified by modifying the applied strain rate, i.e. strain rates of 0.0167 and 1.67 s^{-1} were applied in a standardized Instron® tensile machine.

Additionally, the strain rate was further increased till dynamic conditions. These high strain rate tests were done by the split Hopkinson tensile bar (SHTB) technique [17,18]. For this purpose, the specimen was pinned into slots between two long bars, the input and output bar. The impact of a projectile generates a tensile loading wave at the free end of the input bar and is further propagating along the input bar towards the sample where it interacts with the specimen. Hence, the loading wave is partly reflected back to the input bar and partly transmitted towards the output bar. Strain gauges on the bars measure the strain corresponding with the loading, reflected and transmitted waves. From those waves, the total *force and elongation* history of the tensile sample can be determined based on the principles of 1-dimensional elastic-wave propagation in bars [19]. The dynamic tests were done at strain rates of ±450 and ±900 s^{-1}. As such, the effect of H can be elucidated at crash impact velocities and the impact of H diffusivity can be analyzed on the fracture mode. High speed camera (HSC) images of the deforming sample were taken during the tests to capture fracture initiation and evaluate the fracture mode upon the applied strain rate.

HYDROGEN INDUCED MECHANICAL DEGRADATION

HYDROGEN UPTAKE CAPACITY

The H content was determined by melt extraction after H pre-charging as described above. The H content increased with applied current density, for which an average over 6 samples was given together with the standard deviation in Table 2. The tensile samples were H pre-charged under identical conditions. Therefore, the actual amount of H present in the sample is known when the tensile test started.

Table 2 - Total hydrogen content for different applied current densities.

H content	Air	0.8 mA/cm²	5 mA/cm²	25 mA/cm²
wppm	0.52 ± 0.08	3.77 ± 0.12	4.67 ± 0.11	4.97 ± 0.13

STATIC TENSILE TESTS

The stress-strain curves of the tensile tests performed at strain rates of 0.0167 and 1.67 s^{-1} on uncharged and H pre-charged samples (at 0.8, 5 and 25 mA/cm²) are illustrated in Figures 3 and 4, respectively. The H induced mechanical degradation was determined and summarized for all conditions in Table 3. Generally, HE increases with increasing current density which can be correlated to the higher H content (cf. Table 2) [20]. This is in good agreement with previous results and confirms the correlation between the HE% and the H amount present in the sample [21,22,23,24]. Furthermore, the H susceptibility decreased when the

strain rate was increased. This was attributed to the H diffusion distance which is lower at the higher testing speed [15, 25]. The distance x (cm) over which H can diffuse, can be calculated by taken the square root of the product of the diffusion coefficient D (cm^2/s) and the time t (s) of the test, i.e. $x = (D \times t)^{1/2}$ [14, 25]. Hence, during a test performed at strain rate of 0.0167 s^{-1}, from the onset of deformation till fracture, H could diffuse over approximately 30 mm, whereas at 1.67 s^{-1}, H was just able to diffuse over about 3 mm. A zone characterized by stress concentration ahead of the crack tip is generated during the test where H can diffuse to and hence accelerating H induced failure. When the strain rate was increased, H had a smaller potential to assist the failure process due to the limited distance it can diffuse during this test.

Table 3 - Summary of the HE degrees.

HE%	0.8 mA/cm²	5 mA/cm²	25 mA/cm²
0.0167 s^{-1}	45	58	72
1.67 s^{-1}	27	37	45

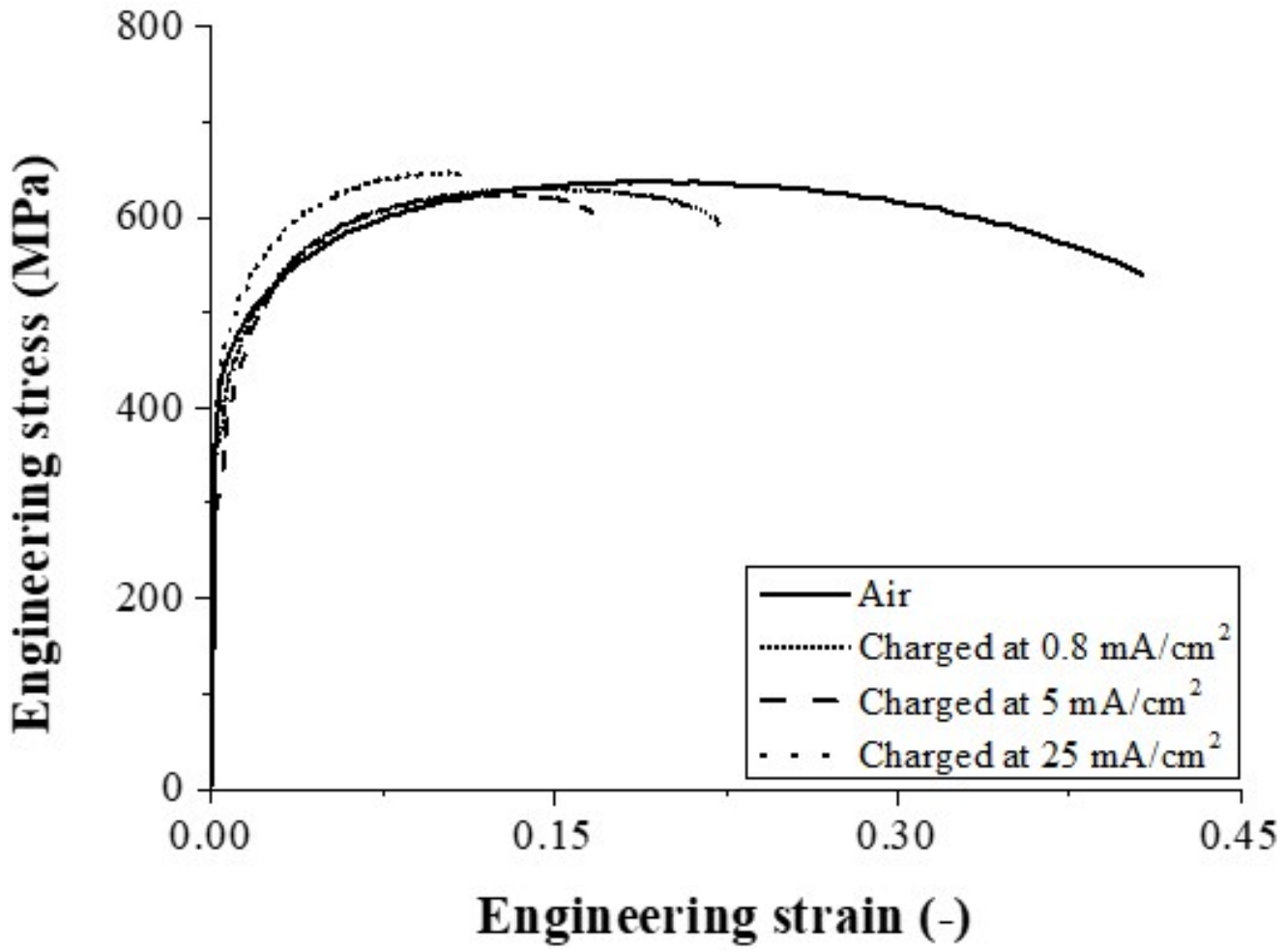

Figure 3 - Engineering stress-strain diagrams of static tensile tests performed at a strain rate of 0.0167 s^{-1}.

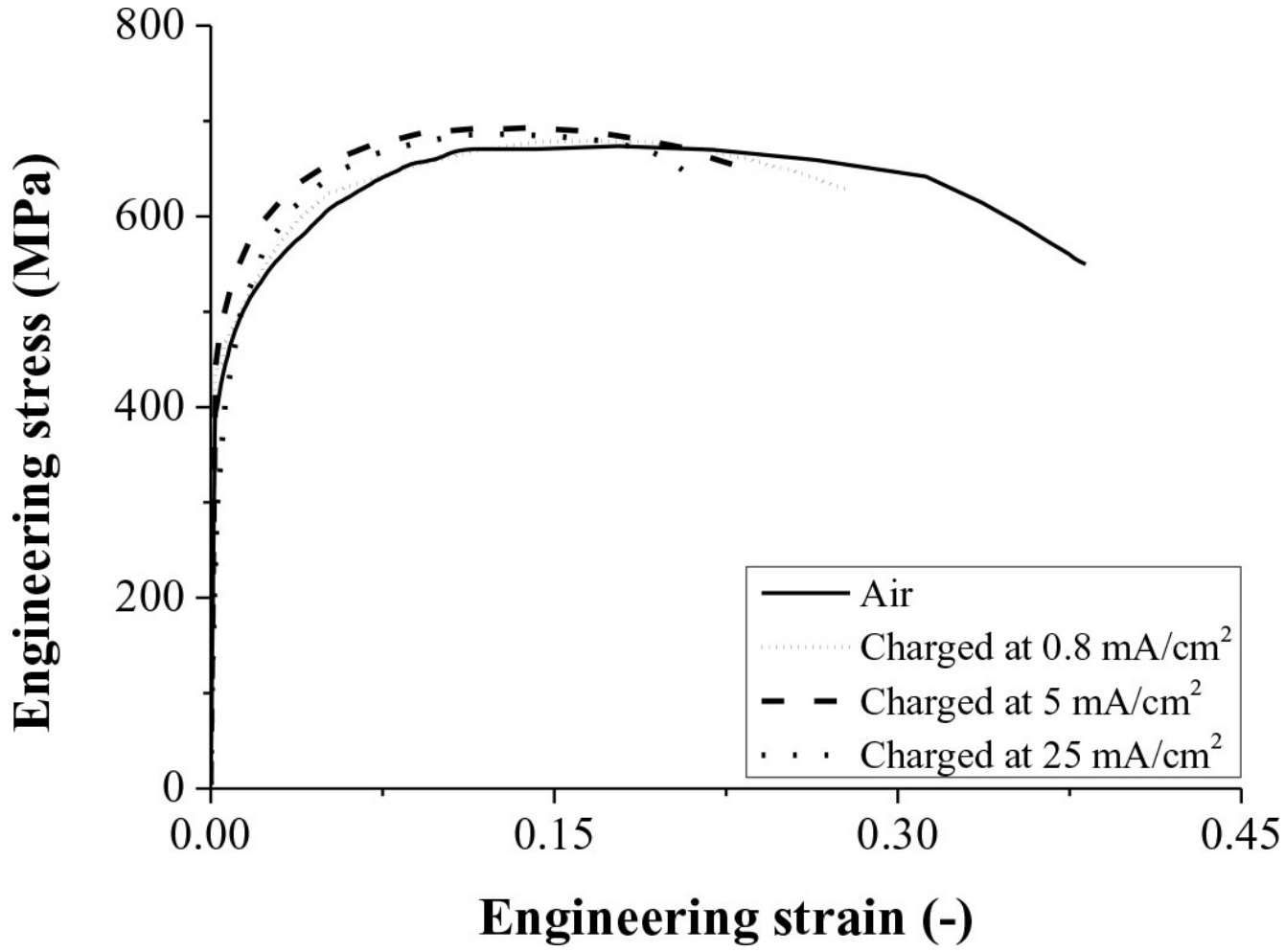

Figure 4 - Engineering stress-strain diagrams of static tensile tests performed at a strain rate of 1.67 s^{-1}

The fracture initiation was captured by HSC images. A sequence of images just before fracture of the tensile test performed at a strain rate of 1.67 s^{-1} on an uncharged sample, is shown in Figure 5. A considerable necking was observed. The fracture initiation was located at the center of the specimen, indicating a ductile failure mode and linked to the high stress triaxiality in the center of the specimen. However, in the H pre-charged (at current density of 5 mA/cm^2) specimen tested at 0.0167 s^{-1}, the fracture initiation occurred at the edge (cf. Figure 6). An increased strain is present during necking at the sample edge and lattice H preferentially diffuses to this zone where it is able to embrittle the material locally, leading to fracture initiation and further accelerated fracture propagation from the edge onwards. This observation was also found for in-situ H charged tensile specimens of DP and TRIP steel, on which failure initiation and propagation was analyzed by electron backscattered diffraction and SEM analysis [4,5,15].

However, when the strain rate was increased to 1.67 s^{-1} after H pre-charging at 0.8 mA/cm^2, a different failure mode was present (cf. Figure 7). Fracture initiation occurred clearly in the center of the specimen, similarly to the tensile test performed on uncharged material (cf. Figure 5). Basically, the fracture initiation was ductile for all tests performed on uncharged samples at both strain rates, while only the H pre-charged samples tested at the higher strain rate of 1.67 s^{-1} showed this ductile failure mode. An overview of the fracture mode for all tests is summarized in Table 4. Therefore, a brittle to ductile transition of fracture initiation was observed as a function of strain rate for H pre-charged samples. This transition in fracture mode when the strain rate was increased can be correlated with a decrease in H diffusion time and hence the H diffusion distance *x*. Zones characterized by stress concentrations ahead of a growing crack tip attract H from the nearby H saturated matrix, which has a higher probability to occur at the slower strain rate. The brittle to ductile transition was observed between the strain rates of 0.0167 s^{-1} and 1.67 s^{-1}, which is linked with a diffusion distance of about 30 and 3 μm, respectively.

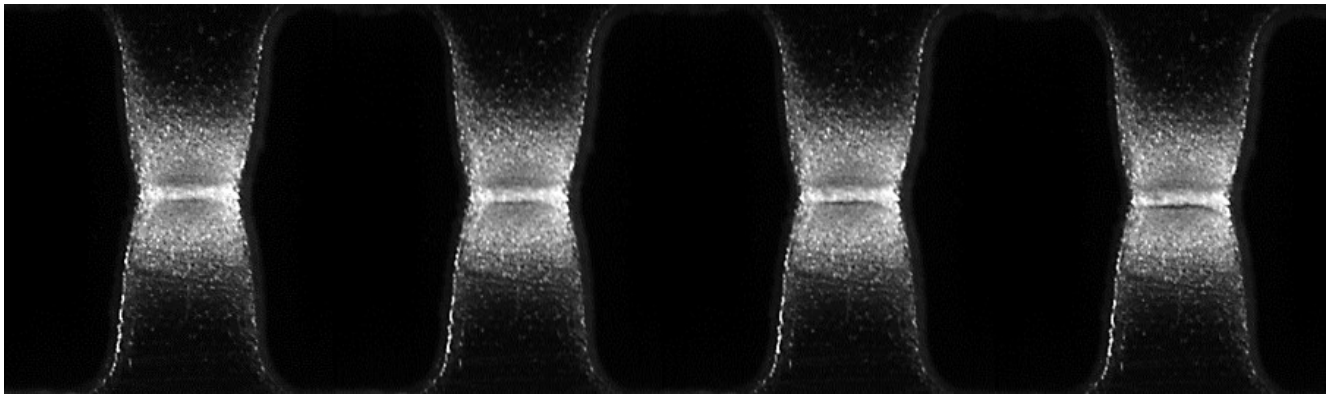

Figure 5 - HSC images of tensile test performed in air at strain rate of 1.67 s^{-1} during fracture.

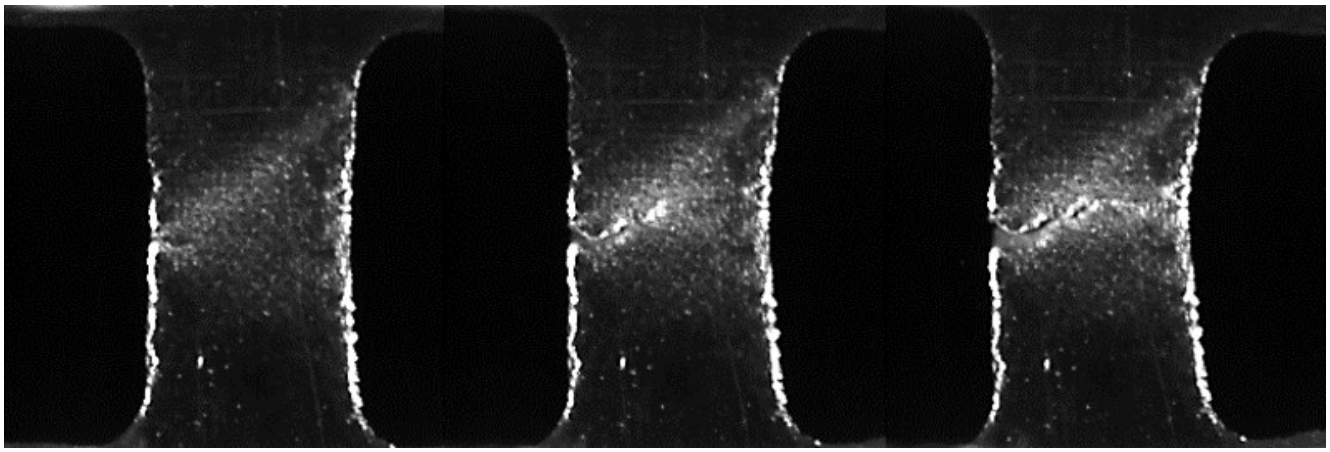

Figure 6 - HSC images of tensile test performed after H pre-charging (5 mA/cm^2) at strain rate of 0.0167 s^{-1} during fracture.

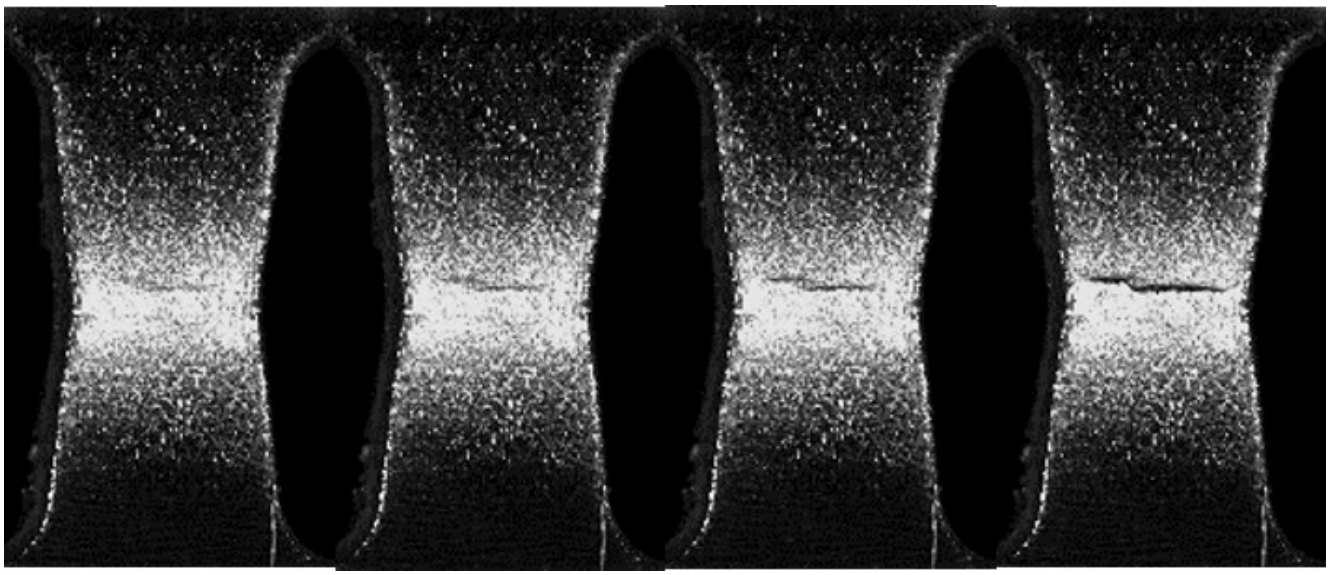

Figure 7 - HSC images of tensile test performed after H pre-charging (0.8 mA/cm^2) at strain rate of 1.67 s^{-1} during fracture.

Table 4 - Overview of fracture modes in the static tensile tests.

Fracture mode	Air	0.8 mA/cm²	5 mA/cm²	25 mA/cm²
0.0167 s^{-1}	Ductile	Brittle	Brittle	Brittle
1.67 s^{-1}	Ductile	Ductile	Ductile	Ductile

DYNAMIC TENSILE TESTS

Figure 8 and 9 display the stress-strain diagrams of SHTB tests performed at a strain rate of 450 and 900 s^{-1}, respectively. The degree of H induced mechanical degradation is summarized in Table 5. Even in these dynamic conditions, a clear impact of H on the mechanical properties was observed as ductility dropped with about 10%. Similarly to the static tests, HE% increased slightly with current density, confirming the correlation between the H content and HE%. Moreover, when the strain rate increased, a slightly lower degree of HE was observed. Correlating this to the diffusion distance *x*, over which H can diffuse during the tensile test, is, however, not relevant since the calculated H diffusion distance was about 0.17 and 0.23 mm at a strain rate of 900 and 450 s^{-1}, respectively.

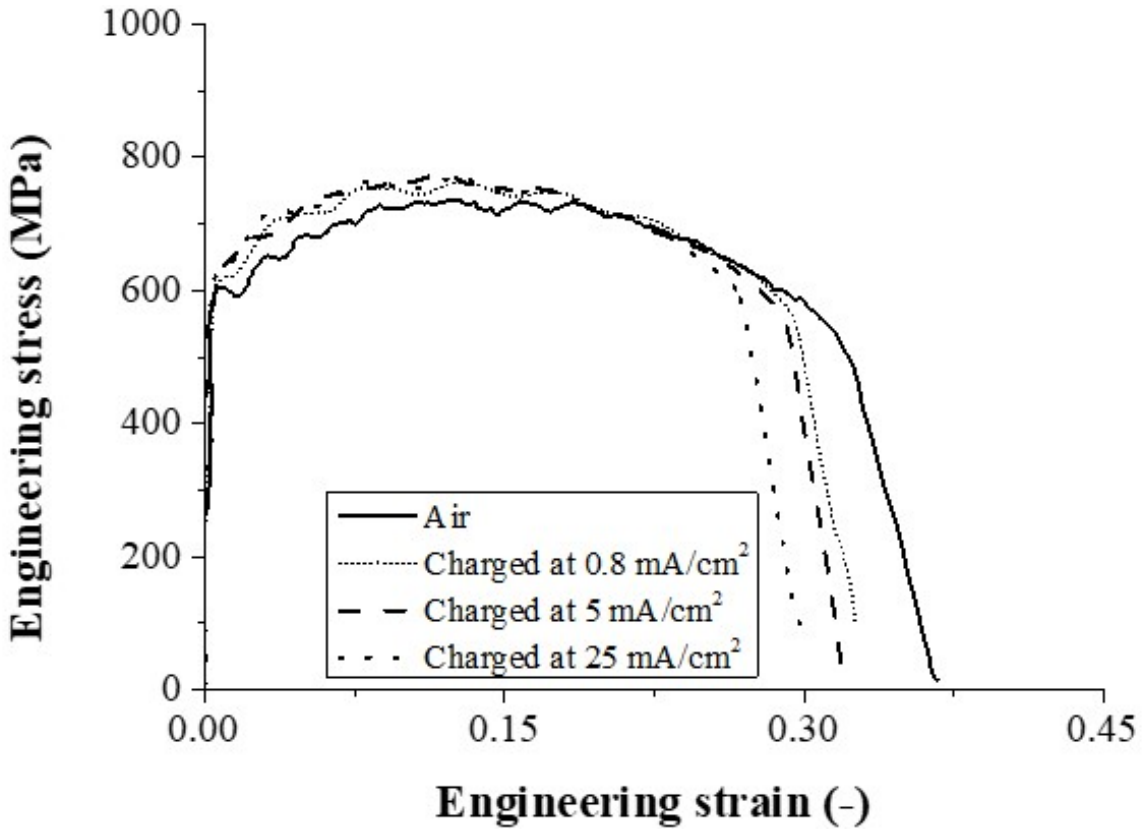

Figure 8 - Engineering stress-strain diagrams of dynamic SHTB tests performed at a strain rate of 450 s^{-1}.

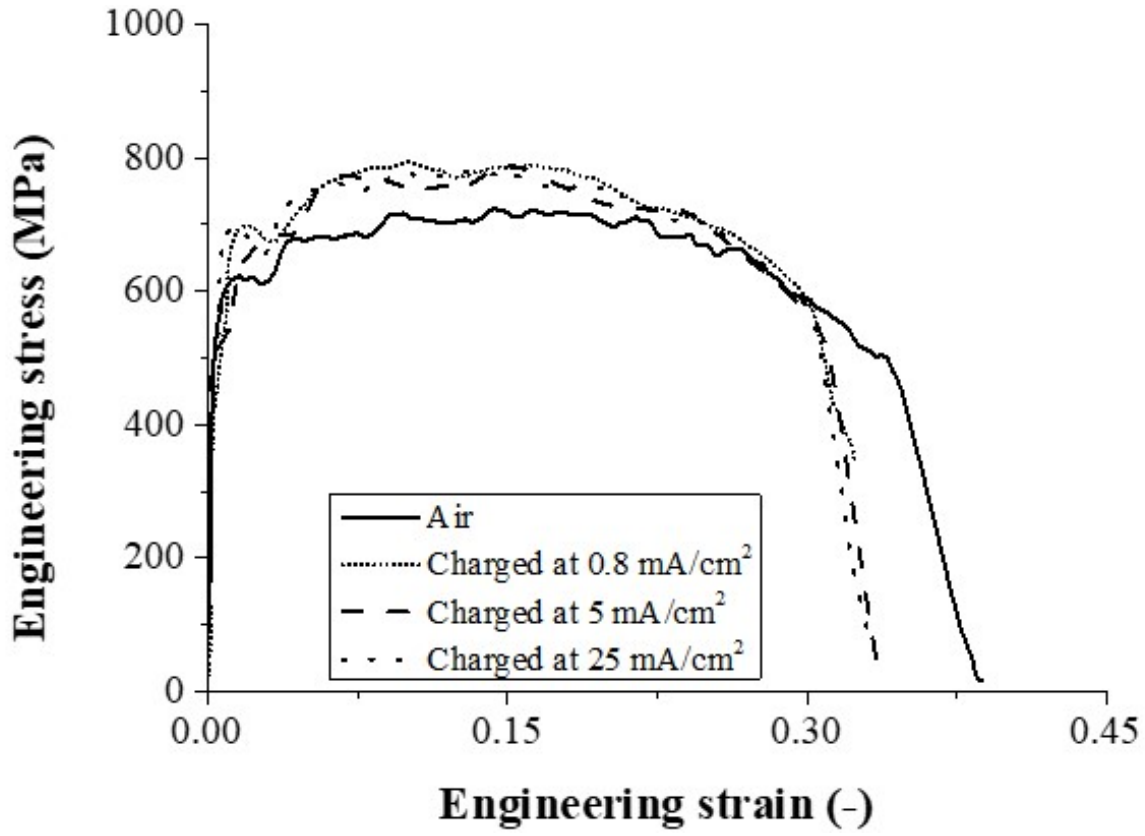

Figure 9 - Engineering stress-strain diagrams of dynamic SHTB tests performed at a strain rate of 900 s^{-1}.

Table 5 - Summary of the HE% for the dynamic tensile test conditions.

HE%	0.8 mA/cm²	5 mA/cm²	25 mA/cm²
450 s^{-1}	9	11	16
900 s^{-1}	8	9	11

FRACTOGRAPHY

All fracture surfaces were studied by SEM and, generally, a ductile dimple pattern was observed. However, a thin brittle zone was present at the center which is correlated to the segregation line of DP steel [15]. The fracture surfaces of two dynamic tests at 450 s^{-1} are presented in Figure 10. A central crack was revealed which size increased with H content. The brittle zone around the crack exhibited some shear characteristics. The crack width increased slightly with increasing strain rate and H content. Figure 11 shows a detailed characterization of the fracture surface of the tensile test performed at 900 s^{-1} after H pre-charging at 5 mA/cm². Second phase particles were observed and EDX analysis revealed the presence of MnS inclusions, which are known to be harmful for HE [15, 26]. The fracture surfaces of the static tensile tests showed similar behavior, i.e. overall dimple ductile surface with cracking and brittle features at the MnS containing segregation central line. However, cleavage was also observed at the center, which was not present for dynamic tests while no extensive cracking was present for these static tests.

This was associated to the synergetic effect of H and the higher triaxialities present in dynamic testing conditions.

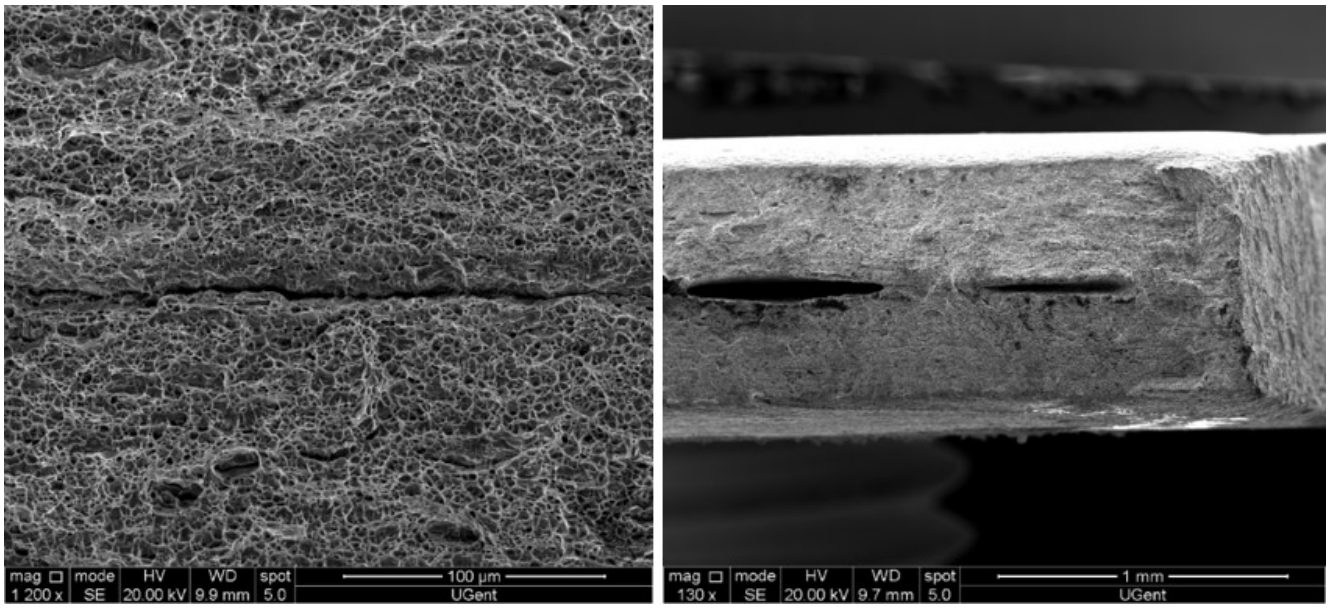

Figure 10 - SEM images of fracture surface of the H pre-charged specimen at 0.8 mA/cm² (left) and at 25 mA/cm² (right), tensile tested at 450 s^{-1}.

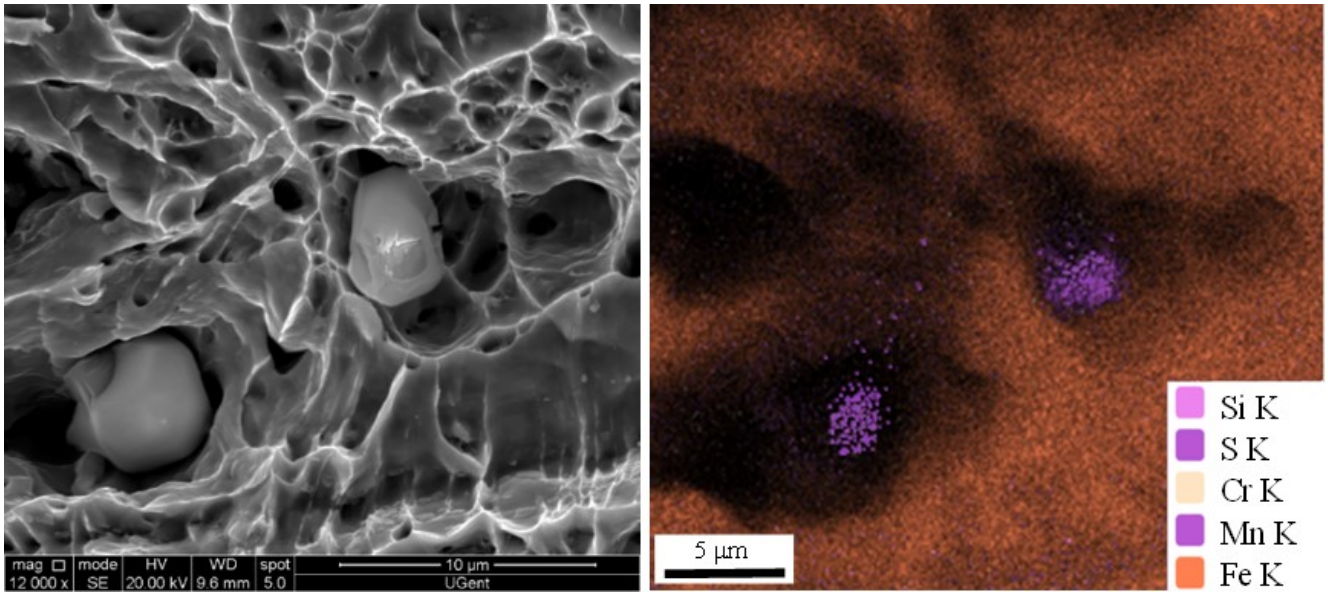

Figure 11 - MnS inclusions in the H induced crack observed on the fracture surface of the H pre-charged specimen at 5 mA/cm², tensile tested at 900 s^{-1}

CONCLUSION

The H induced mechanical degradation in DP steel was studied by performing tensile tests under static and dynamic conditions. The samples were H pre-charged and tensile tests were subsequently done ex-situ. The current density was adjusted to introduce a different amount of H into the samples. The effect of the H diffusivity during the test on the HE sensitivity was estimated by increasing the strain rate from static ($1.67*10^{-2}$ and 1.67 s^{-1}) to dynamic (450 and 900 s^{-1}) conditions. The HE susceptibility increased with applied current density for conditions due to higher amounts of H, as determined by melt extraction. Moreover, the HE degree was increased with slower strain rates. This was linked to higher probability of H to diffuse to regions of stress concentration ahead of a crack tip at slower strain rate and as such accelerating failure. Even at the highest strain rate (900 s^{-1}), the material lost about 10% of its ductility, which was related with H present in the samples and not due to H diffusion during testing. This was concluded since H induced brittle failure initiated at the edges of the samples at slow strain rates. However, at a strain rate of 1.67 s^{-1}, fracture initiated in a ductile way from the center similarly as the tests performed in air. Fractography revealed a brittle central line when H pre-charged, which evolved into a major crack which size increased with applied strain rate. EDX analysis revealed the presence of MnS inclusions in this segregation line, initiating the H induced cracks.

ACKNOWLEDGEMENTS

TD holds a postdoctoral fellowship via grant nr. BOF01P03516. The authors wish to thank the Special Research Fund (BOF), UGent (BOF15/BAS/06). The authors also acknowledge the technical staff from the Department Materials, Textiles and Chemical Engineering and the Department of Electrical Energy, Metals, Mechanical Constructions & Systems, UGent, for their help with experiments and/or sample preparation.

REFERENCES

1. [1] Loidl M, Kolk O, 169, 22-25, 2011, BMW Group, Germany.
2. [2] Ryu JH, Chun YS, Lee CS, Bhadeshia HKDH, Suh DW, Acta Mat, 60, 4085-4092, 2012.
3. [3] Sun J, Jiang T, Sun Y, Wang Y, Liu Y, Journal of Alloys and Compounds, 698, 390-399, 2017.
4. [4] Laureys A, Depover T, Petrov R, Verbeken K, Int Journal of H Energy, 40,16901-16912, 2015.
5. [5] Laureys A, Depover T, Petrov R, Verbeken K, Materials Characterization, 112, 169-179, 2016.
6. [6] Liu Q, Venezuela J, Zhang M, Zhou Q, Atrens A, Corrosion Science, 111, 770-785, 2016.
7. [7] Ronevich JA, Speer JG, Matlock DK, SAE Int Journal Mater Manuf, 3, 255-267, 2010.
8. [8] Depover T, Pérez Escobar D, Wallaert E, Zermout Z, Verbeken K, Int Journal of H Energy, 39, 4647-4656, 2014.
9. [9] Duprez L, Verbeken K, Verhaege M, in Proc. of the Int. Hydrogen Conf., Jackson, Wyoming, 2008.
10. [10] Pérez Escobar D, Verbeken K, Duprez L, Verhaege M, Mat Sci Eng A, 551, 50-58, 2012.
11. [11] Davies RG, Scripta Mat, 17, 889-892, 1983.
12. [12] Gu JL, Chang KD, Fang HS, Bai BZ, ISIJ Int, 42, 1560-1564, 2002.
13. [13] Sun S, Gu J, Chen N, Scripta Mat, 23, 1735-1738, 1989.
14. [14] Koyama M, Tasan CC, Akiyama E, Tsuzaki K, Raabe D, Acta Mat, 70, 174-187, 2014.
15. [15] Depover T, Wallaert E, Verbeken K, Mat Sci and Eng A, 649, 201-208, 2016.
16. [16] Iyer RN, Pickering HW, Zamanzadeh M, Journal of Electrochemical Society, 136, 2463-2470, 1989.
17. [17] Verleysen P, Degrieck J, Int J of Impact Eng, 38, 406-415, 2011.
18. [18] Van Slycken J, Verleysen P, Degrieck J, Bouquerel J, De Cooman BC, Mat Sci and Eng A, 460, 516-524, 2007.
19. [19] Kolsky H, Proc Phys Soc London B, 62, 676-700, 1949.
20. [20] Liu Q, Atrens AD, Shi Z, Verbeken K, Atrens A, Corrosion Science, 87, 239-258, 2014.
21. [21] Depover T, Verbeken K, Corrosion Science, 112, 308-326, 2016.
22. [22] Depover T, Verbeken K, Mat Sci and Eng A, 669, 134-149, 2016.
23. [23] Depover T, Verbeken K, Int Journal of H Energy, 41, 14310-14329, 2016.
24. [24] Depover T, Verbeken K, Mat Sci and Eng A, 675, 299-313, 2016.
25. [25] Depover T, Verbeken K, Mat Sci and Eng A, 664, 195-205, 2016.
26. [26] Pérez Escobar D, Miñambres C, Duprez L, Verbeken K, Verhaege M, Corrosion Science, 53, 3166–3176, 2011.